A Global View of Equatorial Waves and Tropical Cyclogenesis

CARL J. SCHRECK III

Cooperative Institute for Climate and Satellites, North Carolina State University, and NOAA/National Climatic Data Center, Asheville, North Carolina, and Department of Atmospheric and Environmental Sciences, University at Albany, State University of New York, Albany, New York

JOHN MOLINARI

Department of Atmospheric and Environmental Sciences, University at Albany, State University of New York, Albany, New York

ANANTHA AIYYER

Department of Marine, Earth, and Atmospheric Sciences, North Carolina State University, Raleigh, North Carolina

(Manuscript received 6 May 2011, in final form 17 August 2011)

ABSTRACT

This study investigates the number of tropical cyclone formations that can be attributed to the enhanced convection from equatorial waves within each basin. Tropical depression (TD)-type disturbances (i.e., easterly waves) were the primary tropical cyclone precursors over the Northern Hemisphere basins, particularly the eastern North Pacific and the Atlantic. In the Southern Hemisphere, however, the number of storms attributed to TD-type disturbances and equatorial Rossby waves were roughly equivalent. Equatorward of 20°N, tropical cyclones formed without any equatorial wave precursor most often over the eastern North Pacific and least often over the western North Pacific.

The Madden–Julian oscillation (MJO) was an important tropical cyclone precursor over the north Indian, south Indian, and western North Pacific basins. The MJO also affected tropical cyclogenesis by modulating the amplitudes of higher-frequency waves. Each wave type reached the attribution threshold 1.5 times more often, and tropical cyclogenesis was 3 times more likely, within positive MJO-filtered rainfall anomalies than within negative anomalies. The greatest MJO modulation was observed for storms attributed to Kelvin waves over the north Indian Ocean.

The large rainfall rates associated with tropical cyclones can alter equatorial wave–filtered anomalies. This study quantifies the contamination over each basin. Tropical cyclones contributed more than 20% of the filtered variance for each wave type over large potions of every basin except the South Pacific. The largest contamination, exceeding 60%, occurred for the TD band near the Philippines. To mitigate the contamination, the tropical cyclone–related anomalies were removed before filtering in this study.

1. Introduction

Liebmann et al. (1994) found that tropical cyclone development concentrated around the low-level convergence and vorticity anomalies associated with the Madden–Julian oscillation (MJO; Zhang 2005). They argued that any convective system with a period longer than the life span of a tropical cyclone could produce a similar clustering. Such precursors include equatorial Rossby (ER) waves, mixed Rossby–gravity (MRG) waves, Kelvin waves, and tropical depression (TD)-type disturbances, commonly referred to as easterly waves (Bessafi and Wheeler 2006; Frank and Roundy 2006; Schreck et al. 2011, hereafter SMM11). For brevity, all of these features will be referred to as equatorial waves because they reside in equatorial regions and share wavelike properties.

SMM11 examined tropical cyclone precursors over the western North Pacific using rainfall data. Tropical cyclogenesis was attributed to wave-enhanced convection when the wave-filtered rainfall anomaly exceeded

Corresponding author address: Carl J. Schreck III, Cooperative Institute for Climate and Satellites-NC, NOAA/National Climatic Data Center, 151 Patton Ave., Asheville, NC 28801.
E-mail: carl.schreck@noaa.gov

DOI: 10.1175/MWR-D-11-00110.1

a threshold value at the genesis location. SMM11 identified a range of thresholds that produced consistent results. Simply requiring a positive anomaly (equivalent to threshold of 0 mm day^{-1}) was too weak of a threshold because noise from the red background could cause small positive anomalies (Wheeler and Kiladis 1999). At the other extreme, 6 mm day^{-1} was too strict because two-thirds of the tropical cyclones would not be attributed to any wave precursor. Such a result would contradict the link between wave precursors and tropical cyclogenesis found by Liebmann et al. (1994) and numerous synoptic studies (e.g., Riehl 1979, p. 465; Yanai 1961; Heta 1990; Fu et al. 2007). Between these extremes, SMM11 found consistent attribution results for a range of thresholds from 2 to 4 mm day^{-1}.

SMM11 attributed twice as many western North Pacific storms to TD-type disturbances as to ER waves, MRG waves, or Kelvin waves, while the MJO was associated with the fewest storms. These results may be expected to vary for other basins. For example, synoptic studies have attributed nearly all tropical cyclone formations over the eastern North Pacific and Atlantic basins to TD-type disturbances (e.g., Avila and Pasch 1995; Avila et al. 2003). On the other hand, cyclogenesis is less likely to be associated with TD-type disturbances in the Southern Hemisphere where these systems are less common (Roundy and Frank 2004; Frank and Roundy 2006). The MJO convection is strongest over the Indian Ocean and weakest over the Atlantic Ocean (Roundy and Frank 2004; Kiladis et al. 2005). Consistent with this pattern, Frank and Roundy (2006) found only a weak connection between tropical cyclogenesis and MJO activity over the Atlantic. These relationships will be tested by applying the attribution methodology to all tropical cyclone basins.

Although SMM11 attributed fewer storms to convection in the MJO than to any other wave type, they noted that the MJO might influence cyclogenesis more strongly in dynamical fields like low-level vorticity and vertical wind shear. The MJO can also stimulate cyclogenesis by amplifying higher-frequency waves (Nakazawa 1986; Sobel and Maloney 2000; Aiyyer and Molinari 2003, 2008). Zonal convergence associated with the convective phase of the MJO provides a favorable region for wave growth through wave accumulation and contraction. This study will examine the amplitudes of equatorial waves during each phase of the MJO and test the effects on the tropical cyclone attributions.

SMM11 demonstrated that the intense rainfall within tropical cyclones could significantly alter equatorial wave diagnostics. Tropical cyclones accounted for up to 27% of the power in shorter-wavelength westward-propagating waves. This spectrum includes signals from all longitudes. The regional variations of the contamination for each wave type will be examined here. To mitigate the contamination, tropical cyclone–related anomalies will be removed before filtering following SMM11.

This study uses similar datasets and methods as in SMM11, but section 2 will outline some notable differences. The geographical variations in tropical cyclone contamination are explored in section 3. Section 4 presents the basin-by-basin attributions of tropical cyclogenesis for each equatorial wave type. The role of the MJO in modulating tropical cyclogenesis is further investigated in section 5, and section 6 concludes with a discussion of the results.

2. Data and methods

SMM11 identified tropical cyclone tracks using version 1 of International Best Track Archive for Climate Stewardship (IBTrACS; Knapp et al. 2010). This study will use version 3, release 2 of IBTrACS. Version 1 averaged the best-track data from numerous agencies around the globe. Averaging disparate best-track datasets introduced new uncertainties in the best-track data, so it was discontinued after version 2. The newly added World Meteorological Organization (WMO) subset of IBTrACS will be used here. This subset only includes data from the Regional Specialized Meteorological Centers (RSMCs) and Tropical Cyclone Warning Centers (TCWCs) that are sanctioned by the WMO. For example, western North Pacific data are obtained exclusively from the Japanese Meteorological Agency (JMA) with no modifications.

SMM11 defined cyclogenesis as the first time a storm achieved maximum 10-min-sustained winds, averaged among the available agencies, of at least 13 m s^{-1} (25 kt). Tropical cyclone agencies use a variety of methods to estimate maximum sustained winds. They also use different averaging periods (typically 1, 2, or 10 min) to report these winds. For greater consistency, the current study simply defines tropical cyclogenesis as the first position in the WMO subset. SMM11 examined western North Pacific tropical cyclogenesis for 1998–2007. IBTrACS version 3, release 2 includes data through 2009, so this study will take advantage of the additional 2 yr of data. SMM11 also only used storms that developed from May to November over the western North Pacific. This study will use all months over every basin. The inclusion of all months is particularly important over the north Indian Ocean. Vertical shear associated with the Indian monsoon suppresses tropical cyclones in that basin during boreal summer. The annual cycle of tropical cyclone activity in this region peaks once before monsoon onset and then again after its termination (Gray 1968).

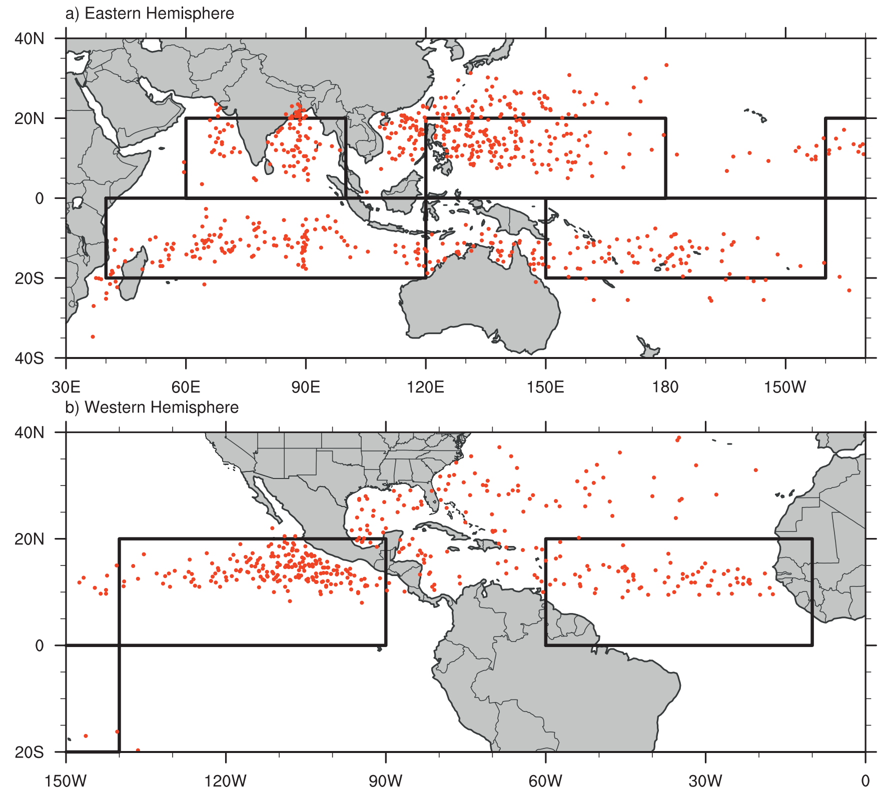

FIG. 1. Genesis locations for 1998–2009. Boxes outline the tropical cyclone basins used in this study: (a) the Eastern Hemisphere and (b) the Western Hemisphere.

Figure 1 shows all genesis locations for 1998–2009. The black boxes outline the tropical cyclone basins adapted from Frank and Roundy (2006). These boxes only extend to 20° latitude to focus on the storms that are most likely to be associated with equatorial waves. Each basin is also defined to be relatively homogeneous. For example, the South China Sea is omitted from the western North Pacific basin because land–ocean contrasts could alter the cyclogenesis process in that region compared with the rest of the basin. In spite of these omissions, the boxes contain the majority of genesis locations over every basin except for the Atlantic. Tropical cyclogenesis occurs more frequently at higher latitudes in that basin, and the omitted Atlantic storms are more likely to have developed in association with extratropical systems (McTaggart-Cowan et al. 2008).

As in SMM11, the equatorial wave–related convection will be identified using filtered Tropical Rainfall Measuring Mission (TRMM) multisatellite rainfall estimates (TRMM product 3B42; Huffman et al. 2007). These data are available from 1998 to the present on 3-hourly 0.25° latitude–longitude grids. They have been averaged to 6-hourly 1° grids for computational efficiency (SMM11). In addition, tropical cyclone–related rainfall has been removed following the method of SMM11. This method uses a weighting function to reduce the anomalies from climatology near each tropical cyclone. The Gaussian weighting function used is

$$w(x, y) = 1 - \exp\left\{-\frac{r(x, y)^2}{2[R(2\ln 2)^{-1/2}]^2}\right\}, \qquad (1)$$

where $r(x, y)$ is the distance from a given grid point to the tropical cyclone's center and R is the radius at half-maximum of the weighting function. Anomalies at the storm's center are reduced to zero, while anomalies at a radius R are reduced by half. We will use $R = 500$ km as in SMM11, but they demonstrated that the attribution results are insensitive to the details of the removal.

SMM11 used the ER, MRG, Kelvin, and MJO filters originally proposed by Wheeler and Kiladis (1999), who were among the first to identify equatorial waves by filtering convective proxies in wavenumber and frequency. The Wheeler and Kiladis (1999) filters encompassed the strongest spectral peaks while also falling between the shallow-water dispersion curves for equivalent depths of 8 and 90 m. Subsequent studies have proposed numerous alternative filters and methods for identifying equatorial waves (e.g., Yang et al. 2003;

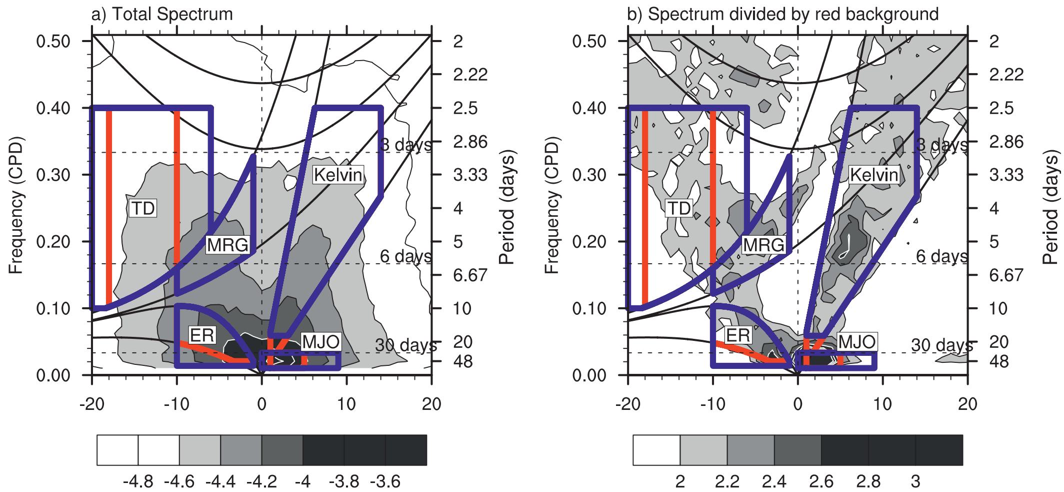

FIG. 2. (a) Total wavenumber–frequency power spectrum for rainfall 15°S–15°N. The base-10 logarithm of the power has been plotted. (b) As in (a), but normalized by a red background as in Roundy and Frank (2004). Blue boxes show the filter bands used in this study, while red boxes indicate the bands used by Schreck et al. (2011).

Roundy and Frank 2004; Kiladis et al. 2005, 2006, 2009; Roundy and Schreck 2009). This study uses expanded filters that include more of the total variance in the wavenumber–frequency spectrum. Consequently, the fraction of all filtered rainfall values that exceed a given threshold increases by as much as 4% with the new filters (not shown). It will be shown that similar attribution results are still found for thresholds from 2 to 4 mm day^{-1} (Fig. 5).

Figure 2a shows the wavenumber–frequency spectrum for rainfall 15°S–15°N, regardless of equatorial symmetry, after the removal of tropical cyclone–related signals. Figure 2b divides this spectrum by an estimate of its red background following Roundy and Frank (2004). The blue boxes outline the filter bands used here, and the red lines identify bands from SMM11. The MRG band is unchanged. The longest period of the Kelvin filter has been reduced from 30 to 17 days to provide more separation from the MJO band (Straub and Kiladis 2002). The MJO band is expanded to include wavenumbers 0–9, as in Kiladis et al. (2005). The low-frequency cutoff in the ER band is extended to 72 days, following Kiladis et al. (2009). Finally, the TD band now includes westward propagation at wavenumbers −20 to −6. Roundy and Frank (2004) and Kiladis et al. (2006) used similar ranges of wavenumbers for their TD filters. The revised filters capture most of the variance that stands out above the red background (Fig. 2b).

One of the primary goals of this study is to evaluate the proportion of genesis events that can be attributed to each wave type in each basin. The significance of these percentages will be evaluated by comparing them with the percentage of *nongenesis* points that also met the attribution criteria. The genesis and nongenesis points should share climatologically similar conditions to make this test as fair as possible. For each storm, we identified nongenesis points that occurred at the same latitude, longitude, month, day, and hour as the genesis point, but fell in different years. For example, if a storm formed at 10°N, 120°E at 0000 UTC 1 June 1998, its corresponding nongenesis points were at 10°N, 120°E at 0000 UTC 1 June during 1999–2009. This approach is similar to that used by Matthews and Kiladis (1999). Once all nongenesis points were identified, we calculated the percentage of their corresponding wave-filtered anomalies that exceeded the attribution threshold for each wave type. Confidence intervals for these percentages were determined using the cumulative density function for a binomial distribution (Wilks 2006, p. 74). If the percentage of storms attributed to a given wave type exceeded the 99% confidence interval, then it was considered to be significant.

3. Contamination by tropical cyclones

Figures 3 and 4 quantify the contamination of the wave-filtered rainfall anomalies by tropical cyclones. The shading represents the total variance, including tropical cyclones, within each filter band. The spatial patterns of these variances resemble those for outgoing longwave radiation and infrared brightness temperature T_b in previous papers (e.g., Kiladis et al. 2009). The contours in Figs. 3 and 4 represent the percentage decrease in the variance caused by removing the storms.

Tropical cyclones contribute more than 20% of the variance (Figs. 3 and 4, dotted contours) in each band

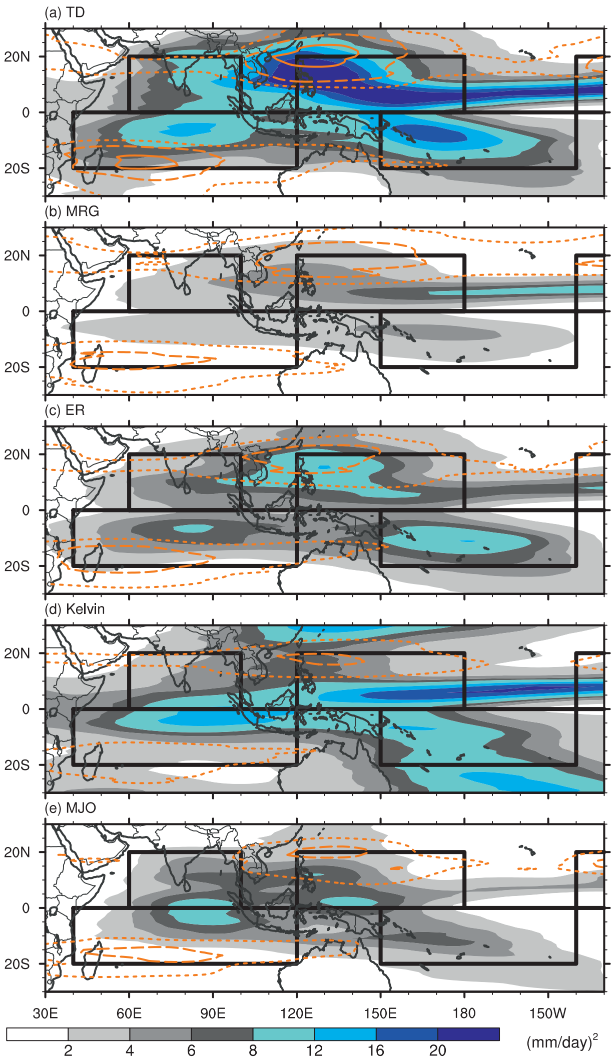

FIG. 3. Filtered variance (shading) in the (a) TD, (b) MRG, (c) ER, (d) Kelvin, and (e) MJO bands. The percentage of variance associated with tropical cyclones in each band is contoured at 20% (dotted), 40% (dashed), and 60% (solid). Boxes outline the tropical cyclone basins used in this study.

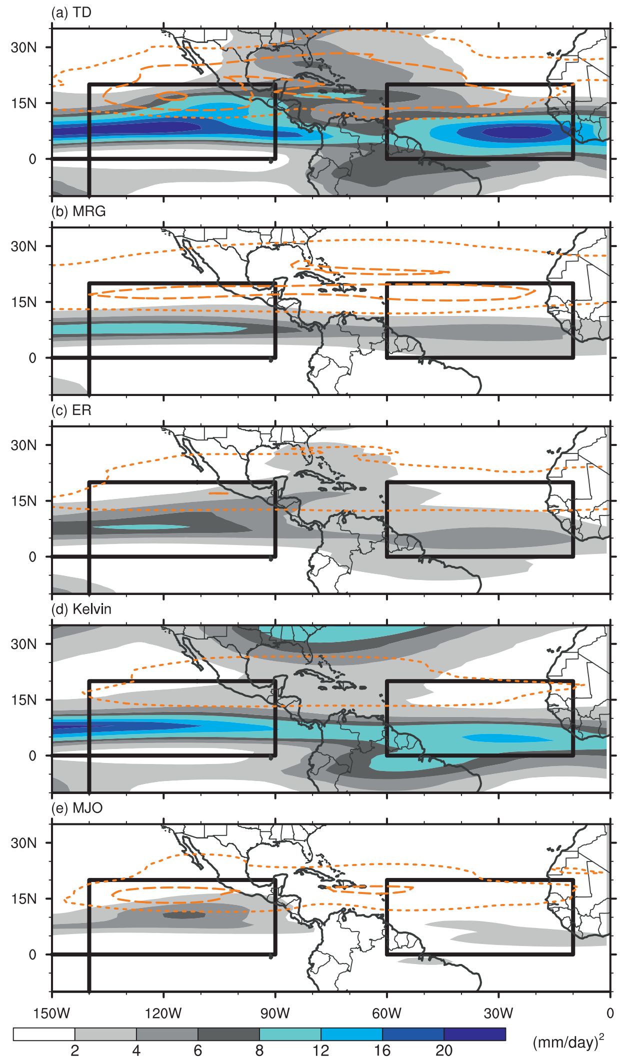

FIG. 4. As in Fig. 3, but focused on the Western Hemisphere.

over broad strips that extend roughly from 15° to 25° latitude. These strips cover large portions of every tropical cyclone basin except the South Pacific, which is less densely populated with tropical cyclones (Fig. 1). In contrast, tropical cyclones are particularly common near the Philippines, and the contamination exceeds 40% for every wave type there (Fig. 3, dashed contours). This region lies poleward of the maximum variance in the MRG, Kelvin, and MJO bands (Figs. 3b,d,e). In the TD and ER bands, however, the 40% contour overlaps with some of the largest total variance observed in these bands (Figs. 3a,c). These variance maxima are therefore substantially attributable to tropical cyclone contamination. The contamination also exceeds 40% over the south Indian Ocean for every wave type except Kelvin waves. It may be less significant in that region, however, as the wave-filtered variances are small there.

SMM11 showed that the TD band in the western North Pacific is particularly vulnerable to tropical cyclone contamination. Figures 3a and 4a confirm that tropical cyclones contribute a larger percentage of the variance in the TD band than in any other band. Tropical cyclone contamination is responsible for more than 60% of the TD variance (solid contours) over portions of the western North Pacific, eastern North Pacific, and south Indian Ocean. Consistent with SMM11, the smallest contamination occurs in the Kelvin band (Figs. 3d and 4d). The contamination only exceeds 40% of the variance near the Philippines. The Kelvin band contains eastward propagation at 9–30 m s^{-1}, but tropical cyclones generally move westward until they reach higher latitudes. It is therefore not surprising that the Kelvin band is more resistant to tropical cyclone contamination than other filter bands.

As with the contamination estimates in SMM11, Figs. 3 and 4 are generally insensitive to the details of the removal method (not shown). The contamination does depend, however, on the dataset chosen. The variance analysis for the Cloud Archive User Service (CLAUS; Hodges et al. 2000; Yang and Slingo 2001) T_b data (not shown) resembles that with the rainfall data (Figs. 3 and 4), but the contamination is generally half as large in T_b compared with rainfall. This difference arises because tropical cyclones can produce rainfall rates an order of magnitude larger than their surroundings. They also produce large anomalies in T_b, but the values are less extreme. Regardless of the dataset, Figs. 3–4 support the findings from SMM11 that tropical cyclone–related anomalies must be removed prior to examining the role of equatorial waves in cyclogenesis.

4. Attribution of tropical cyclogenesis

As in SMM11, tropical cyclogenesis is attributed to an equatorial wave when the filtered rainfall anomaly exceeds a threshold value at the genesis location. Figure 5 shows the percentage of storms attributed to each equatorial wave type using the 2 mm day^{-1} threshold (white bars) and for the 4 mm day^{-1} threshold (gray bars). With either threshold, the percentages can sum to more than 100% because a given storm may be attributed to more than one wave type. The red lines indicate the 99% statistical significance levels based on nongenesis points, as described in section 2. For each wave type, bars that exceed the red line may be considered significant. Note that the percentage of storms not attributed to any wave type (''None'') is always well below the red lines, which confirms that tropical cyclogenesis is more likely to occur when at least one wave type exceeds the attribution threshold.

Figure 5a shows the results for the western North Pacific, which are comparable to those from SMM11. The expansion of the TD, ER, and MJO bands compared with SMM11 increases the number of storms attributed to these wave types by as much as 15% (cf. Figs. 5–9 from SMM11). SMM11 found that each wave type was more likely to reach its attribution threshold at genesis points than at nongenesis points. Consistent with those results, the percentage of western Pacific storms attributed to each wave type in Fig. 5a passes the statistical significance test used here. Also consistent with SMM11, more western North Pacific tropical cyclones are attributed to TD-type disturbances than any other wave type (Fig. 5), and ER waves are the second most important. In contrast to previous results, however, the fraction of storms attributed to the expanded MJO band is now comparable to those attributed to Kelvin and MRG waves.

TD-type disturbances are the primary tropical cyclone precursors over all basins in the Northern Hemisphere (Figs. 5a–d). They are particularly dominant over the eastern North Pacific and the Atlantic basins where fewer storms are attributed to other wave types (Figs. 5b,c). The ER waves are generally second in importance after TD-type disturbances over the Northern Hemisphere basins. In the Southern Hemisphere, however, the numbers of storms attributed to TD-type disturbances and ER waves are roughly equivalent (Figs. 5e,f). MRG waves are attributable for more storms over the western North Pacific, north Indian Ocean, and South Pacific than over other basins. Meanwhile the MRG attributions for the 4 mm day^{-1} threshold are not significant over the eastern Pacific or the south Indian Ocean (Figs. 5b,e). Kelvin waves exert their greatest relative influence on tropical cyclogenesis over the north Indian Ocean (Fig. 5d), while they make no significant contribution to genesis over the eastern Pacific, the Atlantic, and possibly the South Pacific (Figs. 5b,c,f). The MJO is most prominent over the western North Pacific, north Indian, and south Indian basins (Figs. 5a,d,e). The fraction of storms developing without a wave precursor (None) also varied between basins. These storms were least common over the western North Pacific and most common over the eastern North Pacific or the Southern Hemisphere, depending on the threshold.

To better understand the basin-to-basin variations, Figs. 6 and 7 show the genesis locations attributed to each wave type overlaid on the rainfall variance, after removing the tropical cyclone signals, for that filter band. The largest variance falls in the TD band (Figs. 6a and 7a). Consistent with past studies, TD-type disturbances are particularly active over the Atlantic (Gu and Zhang 2001), the eastern North Pacific (Shapiro 1986), and the western North Pacific (Takayabu and Nitta 1993). The large TD variance over the Northern Hemisphere basins helps to explain why TD-type disturbances are the dominant precursors there.

Somewhat weaker TD variance occurs over the Southern Hemisphere basins. Gu and Zhang (2002) identified similar TD-type signals over the South Pacific, but these disturbances have not been extensively studied. Roundy and Frank (2004) attributed this signal to MRG waves whose periods were decreased by background advection. Alternatively, the TD variance over the South Pacific could be associated with the portion of the background variability that falls within the TD filter band. Future studies should analyze this variability to

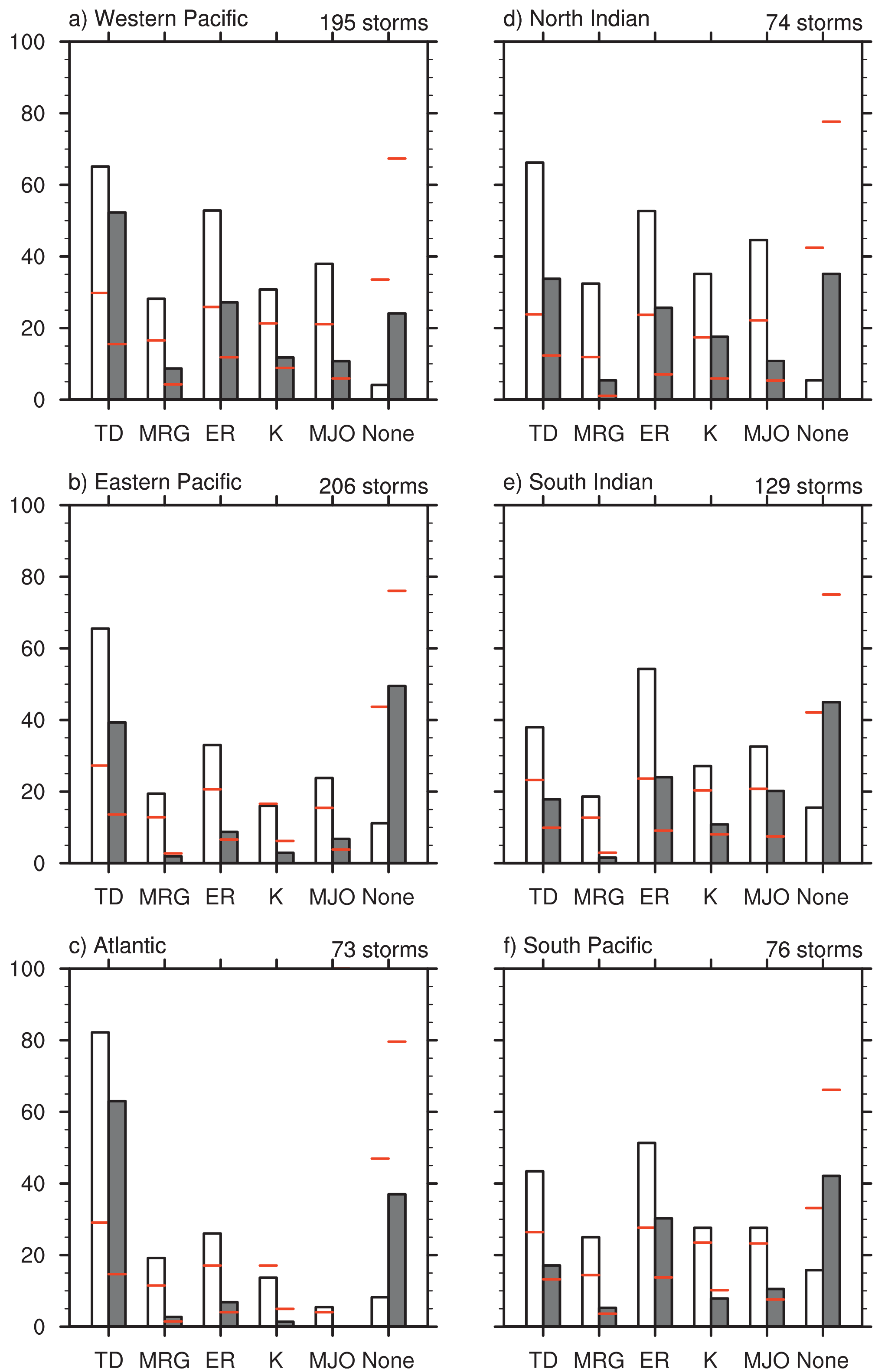

FIG. 5. Percentage of storms attributed to each wave type using thresholds of 2 mm day^{-1} (white bars) and 4 mm day^{-1} (gray bars) in the (a) western North Pacific, (b) eastern North Pacific, (c) Atlantic, (d) north Indian, (e) south Indian, and (f) South Pacific basins. Red lines indicate the 99% significance levels, as described in the text.

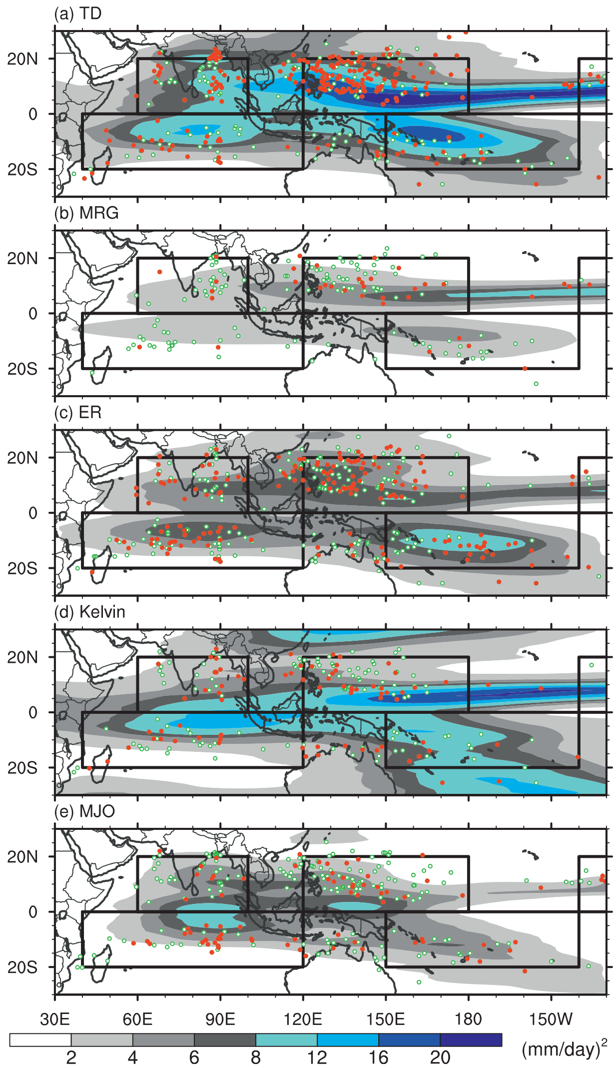

FIG. 6. Genesis locations attributed to (a) TD-type disturbances, (b) MRG waves, (c) ER waves, (d) Kelvin waves, and (e) the MJO overlaid on the variance for the given filter band, following the removal of tropical cyclone–related signals. Green circles identify genesis locations associated with filtered anomalies of 2–4 mm day^{-1}. Red dots identify those exceeding 4 mm day^{-1}. Boxes outline the tropical cyclone basins used in this study.

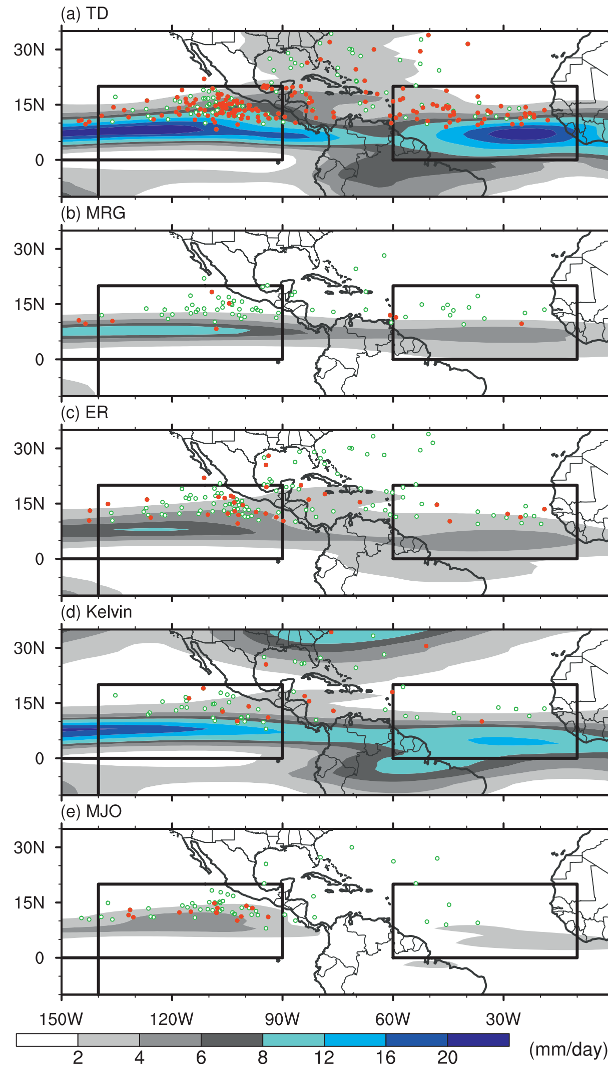

FIG. 7. As in Fig. 6, but focusing on the Western Hemisphere.

determine whether it is associated with real TD-type disturbances.

The spatial pattern of the ER variance (Figs. 6c and 7c) roughly mirrors that of TD-type disturbances (Figs. 6a and 7a). A notable difference is that TD variance peaks in the Northern Hemisphere, while the ER variance maximizes in the Southern Hemisphere. This contrast may explain why TD-type disturbances are the predominant Northern Hemisphere precursor and ER waves are the primary precursor in the Southern Hemisphere (Fig. 5).

The MRG variance peaks over the central North Pacific (Fig. 6b), but most of the tropical cyclones attributed to MRG waves developed northwestward of this maximum. This pattern is consistent with the tropical cyclones developing as the MRG waves turn northwestward off the equator over the western North Pacific (Dickinson and Molinari 2002). The equatorially antisymmetric convection of MRG waves produces a secondary maximum in MRG variance over the South Pacific (Wheeler et al. 2000). The storms attributed to MRG waves over the South Pacific generally develop near the date line associated with this peak in variance. MRG waves are also active over the eastern North Pacific (Fig. 7b), but less than 20% of the storms in that region are attributed to these waves (Fig. 5b). Most eastern North Pacific storms develop northeastward of the maximum MRG variance (Fig. 7b), which may explain why the westward-moving MRG waves have a limited role over this basin.

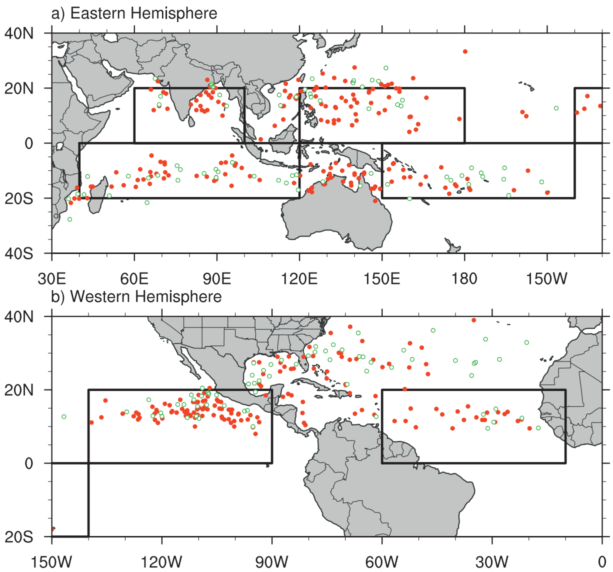

FIG. 8. Genesis locations for storms not attributed to any wave type. Green circles identify genesis locations where all filtered anomalies were less than 2 mm day^{-1}. Red dots denote those where at least one wave type exceeded 2 mm day^{-1} but none exceeded 4 mm day^{-1}. (a) The Eastern Hemisphere and (b) the Western Hemisphere. Boxes outline the tropical cyclone basins used in this study.

Equatorial Kelvin waves and extratropical Rossby waves share similar propagation characteristics and can even interact with each other (Straub and Kiladis 2003a). Extratropical signals likely dominate the Kelvin band poleward of 25° latitude. These signals are particularly prominent over the western North Pacific, the northwestern Atlantic, and the South Pacific convergence zone (Figs. 6d and 7d). Signals within 15° of the equator are primarily associated with actual Kelvin waves. Storms that developed in the intermediate latitudes (15°–25°) require additional analysis to identify the nature of the Kelvin signals. Many of the tropical cyclones attributed to Kelvin waves over the western North Pacific fall into this category.

The MJO variance exhibits two distinct peaks: one over the equatorial Indian Ocean and a second over the equatorial western North Pacific (Fig. 6e). These are also regions with the highest fractions of storms attributed to the MJO (Fig. 5). The storms attributed to the MJO over the south Indian Ocean cluster around the maximum MJO variance in that region. The MJO variance is weakest over the Atlantic (Fig. 7e), which may explain why less than 6% of the storms in that region are attributed to it (Fig. 5c).

SMM11 found that western North Pacific storms not attributed to any wave developed significantly farther poleward than those that had equatorial wave precursors. Figure 8 shows the genesis locations for these storms around the globe. Using the 2 mm day^{-1} threshold (green circles), only 9% (82 of 887) of tropical cyclones developing equatorward of 20° latitude do not have an equatorial wave precursor. This percentage increases to 28% (51 of 182) for storms that develop farther poleward. Similar results are found with the 4 mm day^{-1} threshold (red dots). Based on these results, tropical cyclones that develop poleward of 20° latitude are 3 times as likely to do so without an equatorial wave precursor.

5. Modulation by the MJO

The attribution method only tests the MJO's direct influence on rainfall at the genesis locations. The MJO also affects cyclogenesis by modulating the amplitudes of higher-frequency waves (Nakazawa 1986; Sobel and Maloney 2000; Aiyyer and Molinari 2003). Figure 9 evaluates this modulation. The bars in Fig. 9 indicate the percentage of grid points 20°S–20°N where a given wave's filtered anomaly exceeds 3 mm day^{-1} *and* where the coincident MJO-filtered anomaly is either positive (red bars) or negative (blue bars). Similar results are found for thresholds of 2 or 4 mm day^{-1}. Figure 9a tests all data points (an insignificant fraction of which also happen to be genesis points), and Fig. 9b tests only genesis points.

Figure 9a indicates that all wave types generate larger anomalies during the positive (convective) phase of the MJO than the negative (suppressed) phase. Each wave type is about 1.5 times more likely to exceed 3 mm day^{-1} during the convective phase. For example, only 3.1% of the TD-filtered data exceed 3 mm day^{-1} and occur coincident with negative MJO anomalies. This percentage increases to 4.6% with positive MJO anomalies, even though the MJO band produces equal numbers of positive and negative anomalies.

The differences between the positive and negative phases of the MJO are even more striking for the tropical cyclogenesis data points (Fig. 9b). Consistent with Liebmann et al. (1994) and Frank and Roundy (2006), 3 times as many storms developed within the positive phase of the MJO (75% of the 887 storms) compared with negative phase (25%). This modulation varies for storms attributed to each wave type. For example, only 2.4 times as many storms are attributed to TD-type disturbances during the positive phase compared with the negative phase. The modulation of storms attributed to Kelvin waves is 5 to 1. All of the differences between the positive and negative phases of the MJO in Fig. 9 are statistically significant at the 99% level using a bootstrap test.

Figure 10 examines the regional variations of the MJO's modulation of tropical cyclogenesis. Consistent

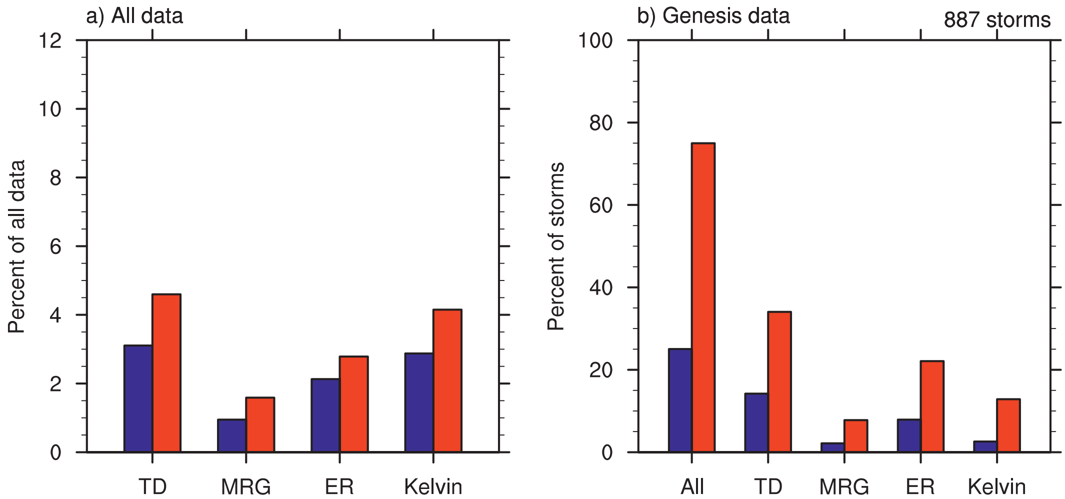

FIG. 9. (a) Percentage of all data between 20°S and 20°N where a given wave exceeds 3 mm day^{-1} and the sign of the MJO-filtered anomaly at the same point is either negative (blue) or positive (red). (b) As in (a), but for data at tropical cyclogenesis locations between 20°S and 20°N.

with Liebmann et al. (1994), the strongest modulation occurs over the western North Pacific and the Indian Ocean. This modulation is particularly strong for storms attributed to MRG waves or ER waves (Fig. 10a). Both of these modulations are nearly 5 to 1. Over the Indian Ocean, similarly strong modulations are observed for storms attributed to Kelvin waves. These patterns are consistent with the findings of Straub and Kiladis (2003b). They showed enhanced MRG activity within the MJO's convection over all basins, but the amplified Kelvin waves were only collocated with the MJO over the Indian Ocean. The MJO produces a 2-to-1 modulation of storms attributed to TD-type disturbances over the eastern North Pacific and the Atlantic. The modulations in these regions are even larger for storms attributed to MRG waves, although they account for less than 10% of the Western Hemisphere tropical cyclone formations.

6. Summary and discussion

SMM11 attributed tropical cyclogenesis to wave-enhanced convection when the wave-filtered rainfall anomaly exceeded a threshold value at the genesis location. This simple definition of attribution omits the dynamical influences of equatorial waves on cyclogenesis, which can be significant. For example, Dunkerton et al. (2009) showed that once a closed vortex forms in a wave-relative frame of reference, it provides a protective envelope that enhances the probability of tropical cyclone development. By using only the rainfall rate to evaluate the role of equatorial waves on tropical cyclogenesis, it is implicitly assumed that tropical cyclones form within areas of convection that coincide with regions of ascent in the shallow-water wave solutions. There is some support for this assumption in case studies (Dickinson and Molinari 2002; Molinari et al. 2007; Schreck and Molinari 2009). Nevertheless, a more complete approach would show the impact of vorticity, vertical wind shear, and other dynamical factors. These fields could be composited in storms that have been attributed to each wave type in this paper. Because that would involve five wave types in six basins, it is left for future work. The following sections will summarize and discuss the attribution results from global and then regional perspectives.

a. Global patterns

SMM11 examined the relative number of western North Pacific tropical cyclones that could be attributed to equatorial waves. This study expanded the results to other basins. The TD-type disturbances were generally the most common tropical cyclone precursor, followed by ER waves. Fewer storms were attributed to MRG waves, Kelvin waves, or the MJO. These global results align with SMM11's findings for the western North Pacific.

The MJO significantly modulates tropical cyclogenesis over every basin (Fig. 9b). These modulations arose in part because the MJO directly alters the environment for tropical cyclogenesis, including deep convection, low-level vorticity, vertical shear, and midlevel moisture (Liebmann et al. 1994; Frank and Roundy 2006; Bessafi and Wheeler 2006; Camargo et al. 2009). The convective envelope of the MJO also provides an environment for growth and accumulation of higher-frequency waves (Nakazawa 1986; Sobel and Maloney 2000; Aiyyer and Molinari 2003, 2008). Figure 9a showed that the other four wave types were 1.5 times more likely to reach the

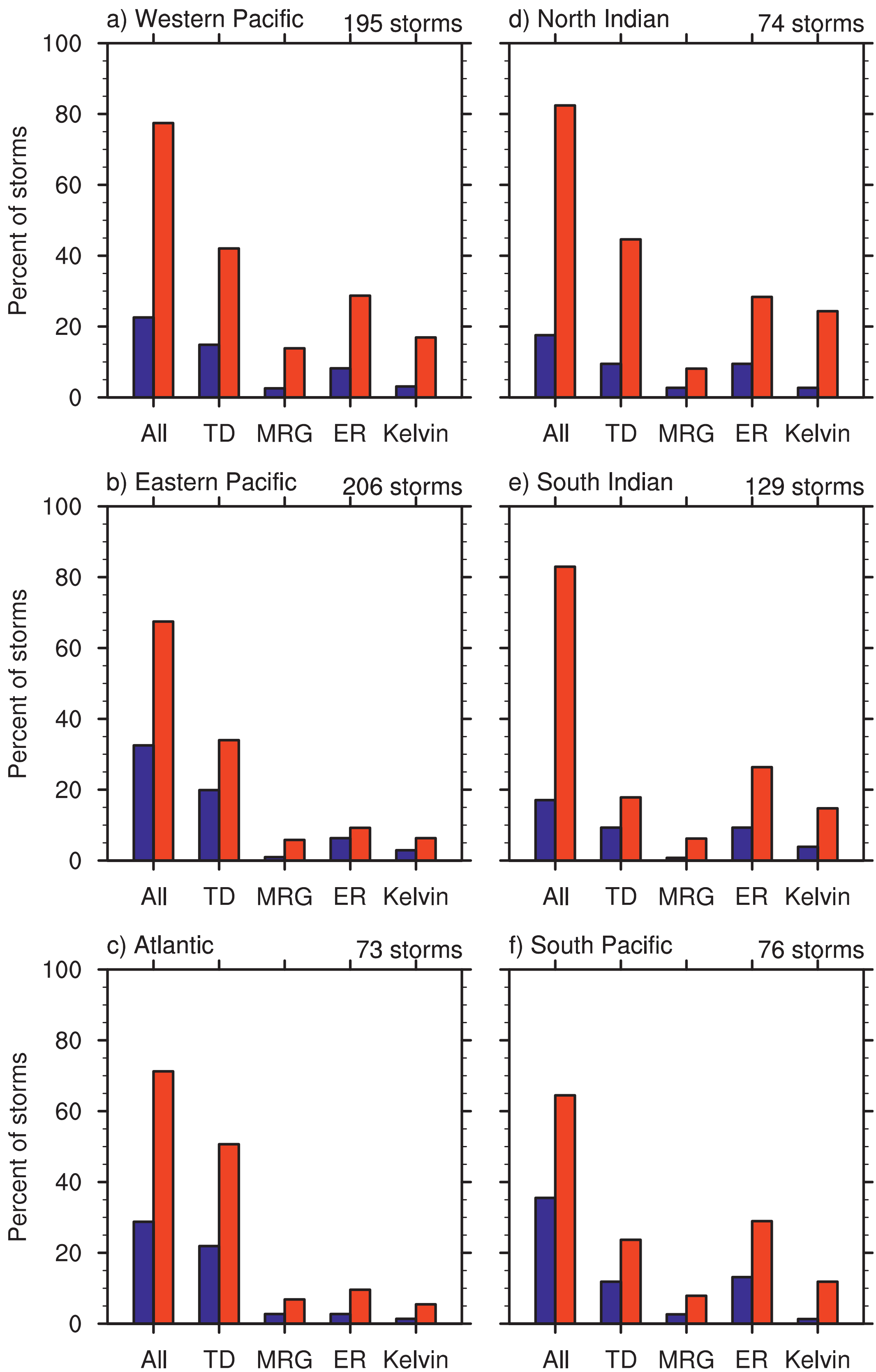

FIG. 10. As in Fig. 9b, but for each basin.

attribution threshold within the positive rainfall anomalies of the MJO. The amplified waves acted as better tropical cyclone precursors. Roughly 3 times more tropical cyclones were attributed to each equatorial wave type during the convective phase of the MJO (Fig. 9b).

Some tropical cyclones formed without any equatorial wave precursors. These storms were 3 times more likely to develop poleward of 20°N (Figs. 6 and 7). In the absence of a wave precursor, tropical cyclones may develop from upper-level troughs (Sadler 1976) or tropical transition (Davis and Bosart 2001). Both of these pathways favor higher latitudes (McTaggart-Cowan et al. 2008).

b. *Regional variations*

1) WESTERN NORTH PACIFIC

Tropical cyclones can form when MRG waves transition to TD-type structures over the western North Pacific (Dickinson and Molinari 2002; Frank and Roundy 2006; Fu et al. 2007). SMM11 found that nearly two-thirds of the western North Pacific storms attributed to MRG waves were also attributed to TD-type disturbances. Using the 4 mm day^{-1} threshold, a greater percentage of storms were attributed to MRG waves over the western North Pacific than any other basin (Fig. 5, gray bars). Western North Pacific tropical cyclones were also more than 5 times as likely to be attributed to MRG waves during the convective phase of the MJO as the suppressed phase (Fig. 10a). Linear shallow-water simulations have suggested that TD-type disturbances develop when MRG waves encounter the equatorial asymmetric background state produced by the MJO over the western North Pacific (Aiyyer and Molinari 2003). This background may be a vital contributor for tropical cyclogenesis from MRG waves.

Previous synoptic studies (e.g., Zehr 1992; Briegel and Frank 1997; Lee et al. 2008) hypothesized that conditions are sufficiently favorable within the western North Pacific monsoon trough to produce tropical cyclones without precursor waves. In this study, fewer storms developed without a wave precursor over the western North Pacific than any other basin (Fig. 5). All the wave types were particularly active in this region (Fig. 6), so it may not be surprising that the majority of storms came from waves. This does not preclude a role for the monsoon trough, however. Tropical cyclogenesis likely occurs when equatorial waves interact with the monsoon trough's favorable background (Frank and Roundy 2006).

2) SOUTHERN HEMISPHERE AND INDIAN OCEAN

TD-type disturbances were the dominant tropical cyclone precursor in each of the Northern Hemisphere basins (Fig. 5). In the Southern Hemisphere, however, ER waves were the most important. These differences may be expected because TD-type disturbances were more active in the Northern Hemisphere, while ER waves were more active in the Southern Hemisphere (cf. Figs. 6a,c). The prominent role of ER waves in Southern Hemisphere tropical cyclogenesis is consistent with previous studies (Bessafi and Wheeler 2006; Leroy and Wheeler 2008; Schreck and Molinari 2009).

Bessafi and Wheeler (2006) showed that the MJO and ER waves significantly modulate tropical cyclogenesis over the south Indian Ocean. They found a smaller though still statistically significant modulation with Kelvin waves, while no significant modulation was found with MRG waves. Consistent with the results, Fig. 5e shows that more tropical cyclone formations were attributed to ER waves and the MJO than to Kelvin waves, and even fewer storms were attributed to the MRG waves.

The percentage of storms attributed to the MJO was largest over the north Indian Ocean, the south Indian Ocean, and the western North Pacific (Fig. 5). Over the north Indian Ocean, 45% of the storms were attributed to the MJO with the 2 mm day^{-1} threshold. The MJO variance is particularly large over these basins (Fig. 6e), which may account for its influence. The MJO's strongest modulation of tropical cyclogenesis, exceeding 4.5:1, occurred over the north and south Indian Oceans (Figs. 10e,f). The modulation was particularly strong for storms attributed to Kelvin waves over the north Indian Ocean. Of these 20 storms, only two developed within negative MJO-filtered rainfall anomalies. When Kelvin waves are embedded within the MJO, they force cyclonic gyres that may act as tropical cyclone precursors (Roundy 2008). In a case study, Schreck and Molinari (2011) found that the MJO might be a key ingredient for tropical cyclones to develop from Kelvin waves. Enhanced Kelvin wave activity is most likely to coincide with the MJO's convective envelope over the Indian Ocean (Straub and Kiladis 2003b), which may account for the MJO's strong modulation of tropical cyclogenesis from Kelvin waves there.

The MJO's modulation of tropical cyclogenesis was less than 2:1 over the South Pacific (Fig. 10f). In contrast, Chand and Walsh (2010) found a 5:1 modulation in that region. While Fig. 10 examined the local MJO-filtered anomalies, they identified the MJO using a global measure: Wheeler and Hendon's (2004) real-time multivariate MJO (RMM) index. Furthermore, Roundy et al. (2009) showed that other signals, such as ER waves and Kelvin waves, could project onto the RMM index. These other signals may account for the differences between Fig. 10f and the results of Chand and Walsh (2010).

3) Western Hemisphere

The dominance of TD-type disturbances as tropical cyclone precursors is greatest over the Atlantic and the eastern North Pacific (Figs. 5b,c). Numerous studies (e.g., Avila and Pasch 1995; Avila et al. 2003) have found that the predominant tropical cyclone precursors in these regions were TD-type disturbances (easterly waves) originating from Africa. As may be expected for these waves, their influence on tropical cyclogenesis was greatest in the main development region of the Atlantic and along the coast of Central America (Fig. 7a).

The MJO variance was weaker in the Western Hemisphere than in the Eastern Hemisphere (Figs. 6e and 7e). Even with the 2 mm day^{-1} threshold, only 5% of Atlantic storms were attributed to the MJO (Fig. 5c). Previous studies (Mo 2000; Barrett and Leslie 2009; Klotzbach 2010; Kossin et al. 2010) have shown that the MJO significantly influences tropical cyclone activity over the Atlantic. These influences are believed to arise from the MJO's impacts on the dynamical factors for tropical cyclogenesis, particularly vertical wind shear. The attribution methodology only accounts for the local enhancement of convection during cyclogenesis, which may explain the weaker relationship observed here.

Over the eastern North Pacific, on the other hand, the MJO was associated with 24% of tropical cyclones using the same threshold (Fig. 5b). Maloney and Hartmann (2000) and Aiyyer and Molinari (2008) have highlighted the MJO's modulation of convection in this region and its impacts on tropical cyclogenesis there. Many of the eastern North Pacific storms attributed to the MJO developed near the Mexican coast (Fig. 7e). Aiyyer and Molinari (2008) showed that the convective phase of the MJO inhibited cyclogenesis farther south in the ITCZ by increasing the vertical shear there, even while it encouraged genesis to the north.

Excluding regions poleward of 20°N, tropical cyclones were most likely to develop without wave precursors over the eastern North Pacific with the 4 mm day^{-1} threshold (Fig. 5, gray bars). Consistent with this pattern, previous studies have downplayed the role of propagating waves over this region (e.g., Maloney and Hartmann 2001; Kerns et al. 2008). Tropical cyclones there might develop from barotropic breakdown of the eastern North Pacific ITCZ without the need for external forcing (Nieto-Ferreira and Schubert 1997).

Numerous storms developed without equatorial wave precursors over the northwestern Atlantic and the Gulf of Mexico (Fig. 8b). McTaggart-Cowan et al. (2008) showed that 28% of Atlantic tropical cyclones developed from extratropical systems. An additional 16% of storms formed from interactions between upper-level troughs and nonbaroclinic low-level disturbances (e.g., TD-type disturbances). Future studies should incorporate extratropical precursors along with the equatorial waves examined here. Determining the relative importance of each of these systems and the potential interactions between them will lead to a more complete understanding of tropical cyclogenesis.

c. *Tropical cyclone signals*

This study quantified the contamination of equatorial wave-filtered rainfall anomalies by tropical cyclones in each basin. Tropical cyclones produced more than 20% of equatorial wave–filtered variance over large portions of every basin except the South Pacific (Figs. 3 and 4, dotted contours). The contamination exceeded 40% in each band near the Philippines. Consistent with SMM11, the TD band was the most susceptible to this contamination, while the Kelvin wave was the least.

Some aspects of equatorial wave activity may need to be reexamined in light of the tropical cyclone contamination. For example, the well-documented storm track of TD-type disturbances near the Philippines (Lau and Lau 1990; Takayabu and Nitta 1993; Chang et al. 1996) also happens to be a preferred storm track for tropical cyclones (Liu and Chan 2008). Figure 3 showed that tropical cyclones contributed more than 60% of the rainfall variance in the TD band over this region. Previous studies identified the TD activity in this storm track with bandpass-filtered T_b (Takayabu and Nitta 1993), 850-hPa meridional winds (Takayabu and Nitta 1993; Chang et al. 1996), or 850-hPa vorticity (Lau and Lau 1990). Tropical cyclones could produce large signals in these fields as well. It might be worthwhile to revisit the climatology of TD-type disturbances with the tropical cyclone signals removed.

Acknowledgments. This research has benefited greatly from conversations with Paul Roundy and Adam Sobel. We thank George Kiladis for his thorough and constructive review. We obtained the rainfall data from the NASA Goddard Distributed Active Archive Center (online at http://disc.sci.gsfc.nasa.gov/data/datapool/TRMM/). We are grateful to David Vollaro and Karen Mohr for their assistance in obtaining and interpolating this data. This work was supported by NSF Grant ATM0839991.

REFERENCES

Aiyyer, A. R., and J. Molinari, 2003: Evolution of mixed Rossby–gravity waves in idealized MJO environments. *J. Atmos. Sci.,* **60,** 2837–2855.

——, and ——, 2008: MJO and tropical cyclogenesis in the Gulf of Mexico and eastern Pacific: Case study and idealized numerical modeling. *J. Atmos. Sci.,* **65,** 2691–2704.

Avila, L. A., and R. J. Pasch, 1995: Atlantic tropical systems of 1993. *Mon. Wea. Rev.,* **123,** 887–896.

——, ——, J. L. Beven, J. L. Franklin, M. B. Lawrence, S. R. Stewart, and J.-G. Jiing, 2003: Eastern North Pacific hurricane season of 2001. *Mon. Wea. Rev.,* **131,** 249–262.

Barrett, B. S., and L. M. Leslie, 2009: Links between tropical cyclone activity and Madden–Julian oscillation phase in the North Atlantic and northeast Pacific basins. *Mon. Wea. Rev.,* **137,** 727–744.

Bessafi, M., and M. C. Wheeler, 2006: Modulation of South Indian Ocean tropical cyclones by the Madden–Julian oscillation and convectively coupled equatorial waves. *Mon. Wea. Rev.,* **134,** 638–656.

Briegel, L. M., and W. M. Frank, 1997: Large-scale influences on tropical cyclogenesis in the western North Pacific. *Mon. Wea. Rev.,* **125,** 1397–1413.

Camargo, S. J., M. C. Wheeler, and A. H. Sobel, 2009: Diagnosis of the MJO modulation of tropical cyclogenesis using an empirical index. *J. Atmos. Sci.,* **66,** 3061–3074.

Chand, S. S., and K. J. E. Walsh, 2010: The influence of the Madden–Julian oscillation on tropical cyclone activity in the Fiji region. *J. Climate,* **23,** 868–886.

Chang, C.-P., J. M. Haywood, P. A. Harr, and L. E. Carr, 1996: Northwestward-propagating wave patterns over the tropical western North Pacific during summer. *Mon. Wea. Rev.,* **124,** 2245–2266.

Davis, C. A., and L. F. Bosart, 2001: Numerical simulations of the genesis of Hurricane Diana (1984). Part I: Control simulation. *Mon. Wea. Rev.,* **129,** 1859–1881.

Dickinson, M., and J. Molinari, 2002: Mixed Rossby–gravity waves and western Pacific tropical cyclogenesis. Part I: Synoptic evolution. *J. Atmos. Sci.,* **59,** 2183–2196.

Dunkerton, T. J., M. T. Montgomery, and Z. Wang, 2009: Tropical cyclogenesis in a tropical wave critical layer: Easterly waves. *Atmos. Chem. Phys.,* **9,** 5587–5646.

Frank, W. M., and P. E. Roundy, 2006: The role of tropical waves in tropical cyclogenesis. *Mon. Wea. Rev.,* **134,** 2397–2417.

Fu, B., T. Li, M. S. Peng, and F. Weng, 2007: Analysis of tropical cyclogenesis in the western North Pacific for 2000 and 2001. *Wea. Forecasting,* **22,** 763–780.

Gray, W. M., 1968: Global view of the origin of tropical disturbances and storms. *Mon. Wea. Rev.,* **96,** 669–700.

Gu, G., and C. Zhang, 2001: A spectrum analysis of synoptic-scale disturbances in the ITCZ. *J. Climate,* **14,** 2725–2739.

——, and ——, 2002: Westward-propagating synoptic-scale disturbances and the ITCZ. *J. Atmos. Sci.,* **59,** 1062–1075.

Heta, Y., 1990: An analysis of tropical wind fields in relation to typhoon formation over the western Pacific. *J. Meteor. Soc. Japan,* **68,** 65–77.

Hodges, K. I., D. W. Chappell, G. J. Robinson, and G. Yang, 2000: An improved algorithm for generating global window brightness temperatures from multiple satellite infrared imagery. *J. Atmos. Oceanic Technol.,* **17,** 1296–1312.

Huffman, G. J., and Coauthors, 2007: The TRMM Multisatellite Precipitation Analysis (TMPA): Quasi-global, multiyear, combined-sensor precipitation estimates at fine scales. *J. Hydrometeor.,* **8,** 38–55.

Kerns, B., K. Greene, and E. Zipser, 2008: Four years of tropical ERA-40 vorticity maxima tracks. Part I: Climatology and vertical vorticity structure. *Mon. Wea. Rev.,* **136,** 4301–4319.

Kiladis, G. N., K. H. Straub, and P. T. Haertel, 2005: Zonal and vertical structure of the Madden–Julian oscillation. *J. Atmos. Sci.,* **62,** 2790–2809.

——, C. D. Thorncroft, and N. M. J. Hall, 2006: Three-dimensional structure and dynamics of African easterly waves. Part I: Observations. *J. Atmos. Sci.,* **63,** 2212–2230.

——, M. C. Wheeler, P. T. Haertel, K. H. Straub, and P. E. Roundy, 2009: Convectively coupled equatorial waves. *Rev. Geophys.,* **47,** RG2003, doi:10.1029/2008RG000266.

Klotzbach, P. J., 2010: On the Madden–Julian oscillation–Atlantic hurricane relationship. *J. Climate,* **23,** 282–293.

Knapp, K. R., M. C. Kruk, D. H. Levinson, H. J. Diamond, and C. J. Neumann, 2010: The International Best Track Archive for Climate Stewardship (IBTrACS). *Bull. Amer. Meteor. Soc.,* **91,** 363–376.

Kossin, J. P., S. J. Camargo, and M. Sitkowski, 2010: Climate modulation of North Atlantic hurricane tracks. *J. Climate,* **23,** 3057–3076.

Lau, K.-H., and N.-C. Lau, 1990: Observed structure and propagation characteristics of tropical summertime synoptic scale disturbances. *Mon. Wea. Rev.,* **118,** 1888–1913.

Lee, C.-S., K. K. W. Cheung, J. S. N. Hui, and R. L. Elsberry, 2008: Mesoscale features associated with tropical cyclone formations in the western North Pacific. *Mon. Wea. Rev.,* **136,** 2006–2022.

Leroy, A., and M. C. Wheeler, 2008: Statistical prediction of weekly tropical cyclone activity in the Southern Hemisphere. *Mon. Wea. Rev.,* **136,** 3637–3654.

Liebmann, B., H. H. Hendon, and J. D. Glick, 1994: The relationship between tropical cyclones of the western Pacific and Indian Oceans and the Madden–Julian oscillation. *J. Meteor. Soc. Japan,* **72,** 401–412.

Liu, K. S., and J. C. L. Chan, 2008: Interdecadal variability of western North Pacific tropical cyclone tracks. *J. Climate,* **21,** 4464–4476.

Maloney, E. D., and D. L. Hartmann, 2000: Modulation of eastern North Pacific hurricanes by the Madden–Julian oscillation. *J. Climate,* **13,** 1451–1460.

——, and ——, 2001: The Madden–Julian oscillation, barotropic dynamics, and North Pacific tropical cyclone formation. Part I: Observations. *J. Atmos. Sci.,* **58,** 2545–2558.

Matthews, A. J., and G. N. Kiladis, 1999: Interactions between ENSO, transient circulation, and tropical convection over the Pacific. *J. Climate,* **12,** 3062–3086.

McTaggart-Cowan, R., G. D. Deane, L. F. Bosart, C. A. Davis, and T. J. Galarneau, 2008: Climatology of tropical cyclogenesis in the North Atlantic (1948–2004). *Mon. Wea. Rev.,* **136,** 1284–1304.

Mo, K. C., 2000: The association between intraseasonal oscillations and tropical storms in the Atlantic basin. *Mon. Wea. Rev.,* **128,** 4097–4107.

Molinari, J., K. Lombardo, and D. Vollaro, 2007: Tropical cyclogenesis within an equatorial Rossby wave packet. *J. Atmos. Sci.,* **64,** 1301–1317.

Nakazawa, T., 1986: Intraseasonal variations of OLR in the tropics during the FGGE year. *J. Meteor. Soc. Japan,* **64,** 17–34.

Nieto-Ferreira, R., and W. H. Schubert, 1997: Barotropic aspects of ITCZ breakdown. *J. Atmos. Sci.,* **54,** 261–285.

Riehl, H., 1979: *Climate and Weather in the Tropics*. Academic Press, 611 pp.

Roundy, P. E., 2008: Analysis of convectively coupled Kelvin waves in the Indian Ocean MJO. *J. Atmos. Sci.,* **65,** 1342–1359.

——, and W. M. Frank, 2004: A climatology of waves in the equatorial region. *J. Atmos. Sci.,* **61,** 2105–2132.

——, and C. J. Schreck, 2009: A combined wave-number–frequency and time-extended EOF approach for tracking the progress of modes of large-scale organized tropical convection. *Quart. J. Roy. Meteor. Soc.,* **135,** 161–173.

——, ——, and M. A. Janiga, 2009: Contributions of convectively coupled equatorial Rossby waves and Kelvin waves to the real-time multivariate MJO indices. *Mon. Wea. Rev.,* **137,** 469–478.

Sadler, J. C., 1976: A role of the tropical upper tropospheric trough in early season typhoon development. *Mon. Wea. Rev.,* **104,** 1266–1278.

Schreck, C. J., and J. Molinari, 2009: A case study of an outbreak of twin tropical cyclones. *Mon. Wea. Rev.,* **137,** 863–875.

——, and ——, 2011: Tropical cyclogenesis associated with Kelvin waves and the Madden–Julian oscillation. *Mon. Wea. Rev.,* **139,** 2723–2734.

——, ——, and K. I. Mohr, 2011: Attributing tropical cyclogenesis to equatorial waves in the western North Pacific. *J. Atmos. Sci.,* **68,** 195–209.

Shapiro, L. J., 1986: The three-dimensional structure of synoptic-scale disturbances over the tropical Atlantic. *Mon. Wea. Rev.,* **114,** 1876–1891.

Sobel, A. H., and E. D. Maloney, 2000: Effect of ENSO and the MJO on western North Pacific tropical cyclones. *Geophys. Res. Lett.,* **27,** 1739–1742.

Straub, K. H., and G. N. Kiladis, 2002: Observations of a convectively coupled Kelvin wave in the eastern Pacific ITCZ. *J. Atmos. Sci.,* **59,** 30–53.

——, and ——, 2003a: Extratropical forcing of convectively coupled Kelvin waves during austral winter. *J. Atmos. Sci.,* **60,** 526–543.

——, and ——, 2003b: Interactions between the boreal summer intraseasonal oscillation and higher-frequency tropical wave activity. *Mon. Wea. Rev.,* **131,** 945–960.

Takayabu, Y. N., and T. Nitta, 1993: 3-5 day-period disturbances coupled with convection over the tropical Pacific Ocean. *J. Meteor. Soc. Japan,* **71,** 221–246.

Wheeler, M., and G. N. Kiladis, 1999: Convectively coupled equatorial waves: Analysis of clouds and temperature in the wave-number–frequency domain. *J. Atmos. Sci.,* **56,** 374–399.

——, and H. H. Hendon, 2004: An all-season real-time multivariate MJO index: Development of an index for monitoring and prediction. *Mon. Wea. Rev.,* **132,** 1917–1932.

——, G. N. Kiladis, and P. J. Webster, 2000: Large-scale dynamical fields associated with convectively coupled equatorial waves. *J. Atmos. Sci.,* **57,** 613–640.

Wilks, D. S., 2006: *Statistical Methods in the Atmospheric Sciences*. 2nd ed. Academic Press, 627 pp.

Yanai, M., 1961: A detailed analysis of typhoon formation. *J. Meteor. Soc. Japan,* **39,** 187–214.

Yang, G.-Y., and J. Slingo, 2001: The diurnal cycle in the Tropics. *Mon. Wea. Rev.,* **129,** 784–801.

——, B. Hoskins, and J. Slingo, 2003: Convectively coupled equatorial waves: A new methodology for identifying wave structures in observational data. *J. Atmos. Sci.,* **60,** 1637–1654.

Zehr, R. M., 1992: Tropical cyclogenesis in the western North Pacific. NOAA Tech. Rep. NESDIS 61, 181 pp.

Zhang, C., 2005: Madden-Julian oscillation. *Rev. Geophys.,* **43,** RG2003, doi:10.1029/2004RG000158.